Doubly Vibrationally Enhanced Four Wave Mixing: The Optical Analog to 2D NMR

Wei Zhao and John C. Wright
Department of Chemistry, University of Wisconsin, Madison, Wisconsin 53706
(Received 21 May 1999)

We report the development of the four wave mixing vibrational analog to 2D NMR and demonstrate its spectral selectivity, sensitivity to the interactions causing mode coupling, and ability to spectrally resolve isotopic mixtures. The method discriminates against uncoupled vibrational modes and isolates the features that are associated with intra- or intermolecular interactions.

PACS numbers: 33.40.+f

Four wave mixing (FWM) spectroscopies like coherent anti-Stokes Raman spectroscopy are based on the interactions that result when three overlapping laser beams induce a nonlinear polarization in a sample which, in turn, drives a fourth output wave [1]. The FWM process is multiplicatively enhanced from the three resonances that result when combinations of the three laser frequencies match spectral transitions in the material. The multiple resonances can provide spectral selectivity when they drive specific molecules or vibrational modes because those transitions are selectively enhanced [2]. Selectivity [3,4] and line narrowing [5] have already been demonstrated for electronic resonances, but there is great interest in developing analogous methods for vibrational resonances [6–9]. Since these methods result in a coherence involving two vibrational modes, they would be the vibrational analog to 2D NMR spectroscopy [10]. High selectivity is possible because the resonances are resolved in two spectral dimensions and because features arising from interactions are selectively enhanced. Two approaches have been suggested for exciting doubly vibrationally enhanced (DOVE) coherences—a six wave mixing (SWM) process where two Raman processes drive the vibrational resonances [6,11] and a FWM process where two infrared lasers drive vibrational resonances directly [7–9]. Both time domain and frequency domain methods are possible for each process. Experimental implementation of DOVE-SWM is hindered by strong interference from two cascaded FWM processes [10–15] but implementation of DOVE-FWM has been conclusively demonstrated [9]. In this paper, we demonstrate the capabilities of DOVE-FWM for achieving 2D vibrational spectroscopy, selectively enhancing specific components in a mixture, and extracting weak spectral features associated with intermolecular interactions.

Figure 1D shows that FWM enhancements can occur through direct infrared absorption (DOVE-IR) or Ramanlike (DOVE-Raman) transitions. Although there are other processes as well, the FWM effects in this paper are dominated by a third order hyperpolarizability γ that is given by

$$\gamma = \sum_{\substack{a,b,c= \\ \text{all states}}} \frac{A^1_{ca}}{(\omega_{ca} - \omega_1 - i\Gamma_{ca})} + \frac{A^2_{ba}}{(\omega_{ba} - \omega_2 + i\Gamma_{ba})} + \frac{A^3_{ba,ca}}{(\omega_{ca} - \omega_1 - i\Gamma_{ca})(\omega_{ba} - \omega_2 + i\Gamma_{ba})} + \frac{A^4_{ba,ca}}{(\omega_{ca} - \omega_1 - i\Gamma_{ca})[\omega_{ba} - (\omega_1 - \omega_2) - i\Gamma_{ba}]} + \frac{A^5_{ba}}{[\omega_{ba} - (\omega_1 - \omega_2) - i\Gamma_{ba}]} + A^6, \quad (1)$$

where ω_{ij} and Γ_{ij} are the frequency difference and dephasing rates for states i and j, ω_n is the frequency of laser n, and A is a proportionality constant [8]. The state and laser labels refer to Fig. 1D. For multiple sample components, the γ_i values add to form the third order susceptibility, $\chi^{(3)} = \sum N_i F \gamma_i$ where F corrects for the local fields and N_i are the concentrations. The output beam intensity at $\omega_4 = \omega_1 - \omega_2 + \omega_3$ depends on $|\chi^{(3)}|^2$ so there are interference cross terms that change the line shapes. The six terms correspond to the different four wave mixing processes and each has three resonances with either electronic or vibrational states. The electronic resonance factors are not shown because the laser frequencies are far from electronic states.

The first two terms in the equation describe singly vibrationally enhanced processes (SIVE) caused by the infrared absorption transition at ω_1 or ω_2 [16], the third term describes the DOVE-IR-FWM process with two infrared absorption transitions, the fourth term describes the DOVE-Raman-FWM process, the fifth term describes ordinary Raman processes, and the last term describes nonresonant processes. The numerators contain four transition moments and electronic factors that control the importance of each contribution. In particular, the transition moments in the DOVE terms must contain at least one factor that involves anharmonicities or nonlinear polarizabilities that couple modes and allow transitions with multiple vibrational quanta changes [3,10,17–20]. These factors are the same as those seen in Raman and infrared combination bands, and it is these transitions that give DOVE methods their unique sensitivity to intra- and intermolecular interactions for FWM and SWM methods [17–20].

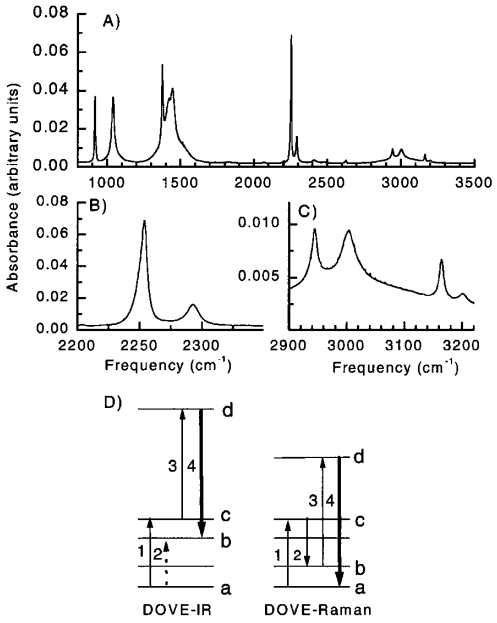

FIG. 1. (A)–(C): Absorption spectra of acetonitrile including expanded regions in the spectral range used for this work. (D) Evolution of coherence for DOVE-IR and DOVE-Raman. Arrows show transitions that cause evolution of the coherences, ρ_{ij}. Numbers label the input frequencies, and letters indicate the states in Eq. (1). Solid arrows show ket evolution, and dotted arrows show bra evolution for ρ_{ij}. The bold arrow is the output ρ_{ij}.

The FWM experiments use a Nd:YAG pumped optical parametric oscillator/amplifier system to generate tunable light near 3100 cm^{-1} for ω_1 and 2250 cm^{-1} for ω_2 as well as the 532 nm ω_3 beam. The output at ω_4 is monitored with filters and a photomultiplier. More details are provided elsewhere [9]. The sample is a 100 μm thick acetonitrile/deuterobenzene mixture where the deuterobenzene's ν_2, $\omega_1 - \omega_2 = 944$ cm^{-1} Raman line provides an internal intensity and frequency standard. Figure 1 shows the acetonitrile absorption spectrum [21]. The important CH_3CN modes for our work are the C≡N stretch at 2253 cm^{-1} (ν_2), the C—H bend at 1372 cm^{-1} (ν_3), a C—C stretch at 918 cm^{-1} (ν_4), the C—H stretches at 2944 and 3003 cm^{-1} (ν_1 and ν_5), and three combination bands at 2293, 3164, and 3200 cm^{-1} corresponding to ($\nu_3 + \nu_4$), ($\nu_2 + \nu_4$), and ($\nu_3 + 2\nu_4$), respectively [22,23]. Our experiments fix ω_2 at different positions near the ν_2 mode and scan ω_1 across the 2900–3300 cm^{-1} region. Under these conditions, term 1 in Eq. (1) could produce peaks at $\omega_1 = 2944$, 3003, 3164, or 3200 cm^{-1} that are independent of ω_2. Term 2 could produce a background that maximizes when $\omega_2 = 2253$ or 2293 cm^{-1}. Term 3 could produce peaks at $\omega_1 = 2944$, 3003, 3164, or 3200 cm^{-1} that maximize when $\omega_2 = 2253$ or 2293 cm^{-1}. Term 4 could produce a peak at $\omega_1 - \omega_2 = 918$ cm^{-1} that maximizes when $\omega_1 = 2944$, 3003, 3164, or 3200 cm^{-1}. Term 5 could produce two peaks at $\omega_1 - \omega_2 = 918$ and 944 cm^{-1} that are independent of ω_2, and term 6 could produce a background that is independent of ω_1 and ω_2.

Figure 2a shows the 2D spectrum of CH_3CN with 8 mole% C_6D_6 [24]. Raman features appear as diagonal ridges since they depend upon $\omega_1 - \omega_2$, the DOVE-Raman features appear as peaks which are sloped along the diagonal since they depend upon ω_1 and $\omega_1 - \omega_2$, and the DOVE-IR features appear as peaks that are oriented along the axes. The spectrum shows two Raman lines that appear as diagonal ridges with $\omega_1 - \omega_2 = 918$ and 944 cm^{-1} [see term 5, Eq. (1)]. The dominant spectral feature is a very strong DOVE-IR peak at $\omega_1 = 3164$ cm^{-1} and $\omega_2 = 2253$ cm^{-1} corresponding to a double resonance with the ν_2 mode and the $\nu_2 + \nu_4$ combination band (see term 3). There is also a weaker DOVE-IR peak at $\omega_1 = 3200$ cm^{-1} and $\omega_2 = 2293$ cm^{-1} corresponding to a double resonance with the $\nu_3 + 2\nu_4$ and $\nu_3 + \nu_4$ combination bands, respectively. It is seen as a distortion in the top part of the feature. These two DOVE-IR features are selective enhancements of the two infrared absorption bands in Fig. 1(C) at 3164 and 3200 cm^{-1}. There are also two DOVE-Raman features that are seen as enhancements of

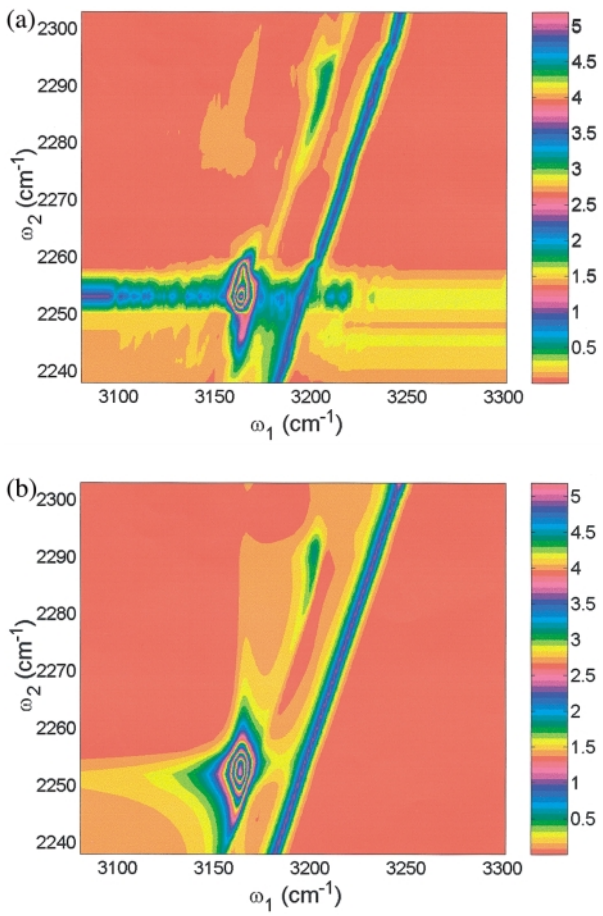

FIG. 2 (color). (a) 2D DOVE spectrum of CH_3CN with 8 mole% C_6D_6. The color scale repeats 4 times to see the weakest features. (b) Theoretical model using Eq. (1).

the 918 cm^{-1} Raman line when $\omega_1 = 3164$ or 3200 cm^{-1} (see term 4). In both cases, the DOVE-Raman feature passes through the region of the DOVE-IR features so there are interference effects that change their line shapes. The two DOVE Raman features correspond to double resonances between ν_4 and either the $\nu_2 + \nu_4$ or $\nu_3 + 2\nu_4$ combination bands. There may also be a weak SIVE band that appears as a horizontal ridge at $\omega_2 = 2253$ cm^{-1} (see term 2).

Figure 2(b) models the 2D spectrum using Eq. (1) and the parameter values in Table I. The modeling reproduces the major features and provides estimates for the different processes. There are differences. The experimental DOVE-IR feature is sharper and disappears more quickly with ω_1 and ω_2 detuning that the modeling predicts. Further work is required to understand this behavior but we believe it is caused by the inhomogeneous broadening contributions that have not been included in the model. The line shape is not purely Lorentzian as we assume and there may be line-narrowing effects that reduce the inhomogeneous broadening [8]. There are also baseline differences that may reflect interference from the windows.

It is important to point out that despite the strength of the C—H absorption lines, the spectra do not contain appreciable DOVE contributions from the ν_1 or ν_5 modes. This mode selectivity is one of the key features of DOVE methods because it spectrally isolates the features that are associated with interactions. The absence of the C—H DOVE cross peaks reflects the absence of interactions associated with anharmonic or nonlinear polarizabilities that could lead to coupling between ν_2 and either ν_1 or ν_5.

The cross-peak intensities observed in this study correlate with the vibrational relaxation processes observed by Deak and co-workers [22,25]. They found that excitation of the C—H stretch mode relaxed dominantly to the ν_3 mode and did not couple with the ν_2 mode. On the other hand, excitation of the $\nu_2 + \nu_4$ combination band showed strong coupling to the ν_2 mode. The intensities also can be understood using the theories for DOVE mode coupling processes where one of the four transitions in FWM must involve a two vibrational quantum change [17–20]. In our work, the DOVE peaks occur because the two quantum change occurs in the combination band excitation, e.g., $\nu_2 + \nu_4$. The selective enhancement of the combination bands is the signature for the mode selectivity of the DOVE methods.

A key feature of DOVE methods is the ability to selectively enhance the features of components or conformers in a complex mixture. To demonstrate this capability, an equal molar mixture of CH_3CN and CD_3CN was prepared with 13 mole % C_6D_6 as an internal standard. The ν_2 and $\nu_2 + \nu_4$ modes in CD_3CN are shifted to 2262 and 3090 cm^{-1}, respectively. Figure 3 shows a series of three ω_1 scans with ω_2 values set for the CH_3CN ν_2 mode at 2253 cm^{-1}, the CD_3CN ν_2 mode at 2262 cm^{-1}, and off-resonance at 2260 cm^{-1}. The changes show the strong component selectivity. The line on the right is the C_6D_6 Raman line which is quite strong because of its higher concentration. Resonance with either the CH_3CN or CD_3CN ν_2 mode results in such large enhancements that the other component's line is not seen. When ω_2 is between the two, both lines appear weakly. Clearly, there is a strong enhancement of either isotopic component depending upon which resonance is chosen by the ω_2 selection.

There are also correlation methods that provide 2D vibrational spectra. These methods are based on the changes that occur in 1D spectra because of external perturbations such as temperature or pressure [26]. Statistical methods transform the data into a 2D format that visualizes correlated changes. In particular, recent femtosecond laser pump-probe methods have used the correlations to create a 2D vibrational spectrum using transient hole burning where bleaching of one mode causes changes in the spectra of the other modes [27,28]. The 2D-DOVE methods do not rely on correlating spectral changes but on the presence of double vibrational coherences requiring mode coupling. They are analogous to the double quantum spin coherences in 2D NMR.

Mukamel proposed a time domain SWM method for 2D vibrational spectroscopy that used Raman instead of infrared transitions to drive the vibrational transitions [6], but experimental frequency domain experiments found that cascaded FWM prevented observation [11]. Later time domain experiments reported SWM [10,12,13] but there is recent evidence that these experiments were also compromised by cascaded FWM [14,15]. Since FWM is the lowest order nonlinear spectroscopy for an isotropic material, it is not subject to interfering lower order cascaded processes.

The potential strengths of DOVE methods is their inherent sensitivity to the intra- and intermolecular interactions that define structural relationships and their ability to selectively enhance particular molecules or

TABLE I. Relative peak values for terms in Eq. (1). The values represent A/Γ for terms 1, 2, and 5, $A/\Gamma_i\Gamma_j$ for terms 3 and 4, and A^6 for term 6. The C_6D_6 internal standard is fixed at 1.

	Term 1	Term 2	Term 3	Term 4	Term 5	Term 6
States		ν_2	$\nu_2, \nu_2 + \nu_4$	$\nu_2 + \nu_4, \nu_4$	ν_4	CH_3CN
Peak inten.	0	0.02	0.19	0.04	0.02	0.013
States			$\nu_3 + \nu_4, \nu_3 + 2\nu_4$	$\nu_3 + 2\nu_4, \nu_4$	C_6D_6 ν_2	C_6D_6
Peak inten.			0.04	0.045	1.000	0.04

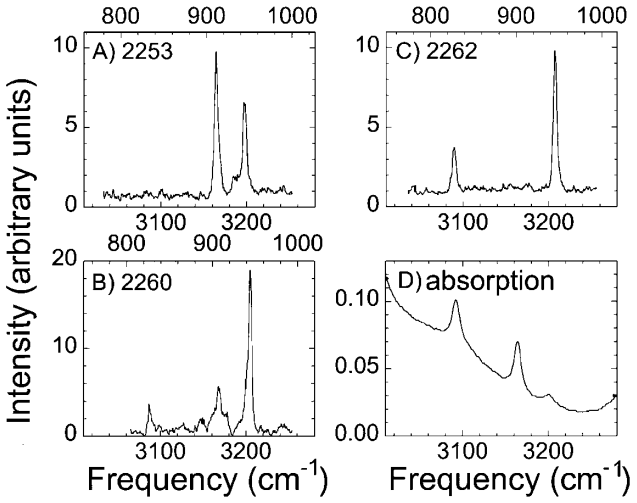

FIG. 3. Scans of ω_1 for 43.5:43.5:13 mole % CH_3CN: CD_3CN: C_6D_6 mixture. The bottom axes show ω_1 and the top axes show $\omega_1 - \omega_2$. The $\omega_2 = 2253$ and 2262 cm^{-1} spectra correspond to resonances with ν_2 of CH_3CN and CD_3CN, respectively. The absorption spectrum is shown for comparison.

conformers in complex samples [2,8–10,29]. Since cross peaks are absent without interactions [10,18–20], DOVE methods have the ability to eliminate much of the spectral congestion in complex samples and isolate the features that are coupled by interactions. The cross-peak intensity reflects similar information to the combination and overtone bands that are usually hidden by the stronger fundamentals. It can also provide direct information about the mode coupling that controls the vibrational energy flow in chemical processes [22,25]. The 2D vibrational and NMR methods are potentially complementary because NMR spectra reflect time-averaged correlations over millisecond spin dephasing times, whereas DOVE spectra reflect the correlations over picosecond vibrational dephasing times. These capabilities should be particularly important for environmental and biochemical systems where the identification of interacting moieties plays a fundamental role in understanding structure/function relationships. For example, it will be interesting to use DOVE methods to study C═O and N—H stretch modes in proteins where H bonding causes mode coupling that might allow one to identify the interacting moieties [30], much as 2D NMR does.

This work was supported by the National Science Foundation under Grant No. CHE-9816829.

[1] J. L. Oudar and Y. R. Shen, Phys. Rev. A **22**, 1141 (1980).
[2] J. C. Wright *et al.*, Int. Rev. Phys. Chem. **10**, 349 (1991).
[3] R. J. Carlson and J. C. Wright, J. Chem. Phys. **92**, 5186 (1990).
[4] J. K. Steehler and J. C. Wright, J. Chem. Phys. **83**, 3188 (1985).
[5] G. B. Hurst and J. C. Wright, J. Chem. Phys. **95**, 1479 (1991).
[6] Y. Tanimura and S. Mukamel, J. Chem. Phys. **99**, 9496 (1993).
[7] A. Zilian, M. J. LaBuda, J. P. Hamilton, and J. C. Wright, J. Lumin. **60&61**, 655 (1994).
[8] J. C. Wright *et al.*, Appl. Spectrosc. **51**, 949 (1997).
[9] W. Zhao and J. C. Wright, Phys. Rev. Lett. **83**, 1950 (1999).
[10] A. Tokmakoff *et al.*, Phys. Rev. Lett. **79**, 2702 (1997).
[11] J. E. Ivanecky and J. C. Wright, Chem. Phys. Lett. **206**, 437 (1993).
[12] K. Tominaga and K. Yoshihara, Phys. Rev. Lett. **74**, 3061 (1995).
[13] T. Steffen and K. Duppen, Phys. Rev. Lett. **76**, 1224 (1996).
[14] D. A. Blank, L. J. Kaufman, and G. R. Fleming, J. Chem. Phys. **111**, 3105 (1999).
[15] D. J. Ulness, J. C. Kirkwood, and A. C. Albrecht, J. Chem. Phys. **108**, 3897 (1998).
[16] M. J. Labuda and J. C. Wright, Phys. Rev. Lett. **79**, 2446 (1997).
[17] M. Cho, K. Okumura, and Y. Tanimura, J. Chem. Phys. **108**, 1326 (1998).
[18] K. Okumura and Y. Tanimura, J. Chem. Phys. **106**, 1687 (1997).
[19] V. Chernyak and S. Mukamel, J. Chem. Phys. **108**, 5812 (1998).
[20] K. Okumura and Y. Tanimura, J. Chem. Phys. **107**, 2267 (1997).
[21] J. E. Bertie and Z. Lan, J. Phys. Chem. B **101**, 4111 (1997).
[22] J. C. Deak, L. K. Iwaki, and D. D. Dlott, Chem. Phys. Lett. **293**, 405 (1998).
[23] P. Venkateswarlu, J. Chem. Phys. **19**, 293 (1951).
[24] M. D. Levenson and N. Bloembergen, J. Chem. Phys. **60**, 1323 (1974).
[25] J. C. Deak, L. K. Iwaki, and D. D. Dlott, J. Phys. Chem. A **102**, 8193 (1998).
[26] I. Noda, Appl. Spectrosc. **47**, 1329 (1993).
[27] P. Hamm, M. Lim, and R. M. Hochstrasser, J. Phys. Chem. B **102**, 6123 (1998).
[28] P. Hamm, M. Lim, W. F. DeGrado, and R. M. Hochstrasser, Proc. Natl. Acad. Sci. U.S.A. **96**, 2036 (1999).
[29] P. C. Chen *et al.*, Appl. Spectrosc. **52**, 380 (1998).
[30] D. Zimdars *et al.*, Phys. Rev. Lett. **70**, 2718 (1993).